

# Flux-dependent occupations and occupation difference in geometrically symmetric and energy degenerate double-dot Aharonov-Bohm interferometers

Salil Bedkihal<sup>1</sup>, Malay Bandyopadhyay<sup>2</sup>, Dvira Segal<sup>1</sup>

<sup>1</sup>*Chemical Physics Theory Group, Department of Chemistry,*

*University of Toronto, 80 Saint George St. Toronto, Ontario, Canada M5S 3H6*

<sup>2</sup>*School of Basic Sciences, Indian Institute of Technology Bhubaneswar, 751007, India*

(Dated: September 23, 2018)

We study the steady-state characteristics and the transient behavior of the nonequilibrium double-dot Aharonov-Bohm interferometer using analytical tools and numerical simulations. Our simple setup includes noninteracting degenerate quantum dots that are coupled to two biased metallic leads at the same strength. A magnetic flux  $\Phi$  is piercing the setup perpendicularly. As we tune the degenerate dots energies away from the symmetric point we observe four nontrivial magnetic flux control effects: (i) flux dependency of the dots occupation, (ii) magnetic flux induced occupation difference between the dots, at degeneracy, (iii) the effect of “phase-localization” of the dots coherence holds only at the symmetric point, while in general both real and imaginary parts of the coherence are nonzero, and (iv) coherent evolution survives even when the dephasing strength, introduced into our model using Büttiker probe, is large and comparable to the dots energies and the bias voltage. Moreover, not only finite dephasing strength does not destroy the coherence features, it can provide new type of coherent oscillations. These four phenomena take place when the dots energies are gated, to be positioned away from the symmetric point, demonstrating that the combination of bias voltage, magnetic flux and gating field, can provide delicate controllability over the occupation of each of the quantum dots, and their coherence.

PACS numbers: 73.23.-b, 85.65.+h, 73.63.-b

## I. INTRODUCTION

The steady-state properties of the Aharonov-Bohm (AB) interferometer have been intensively investigated<sup>1,2</sup>, with the motivation to explore coherence effects in electron transmission within mesoscopic and nanoscale structures<sup>3,4</sup>. Particularly, the role of electron-electron (e-e) interaction effects in AB interferometry has been considered in Refs.<sup>5–11</sup>, revealing, e.g., asymmetric interference patterns<sup>5</sup> and the enhancement<sup>10</sup> or elimination<sup>12</sup> of the Kondo physics. Recent works further considered the possibility of magnetic-field control in molecular transport junctions<sup>13–16</sup>. The real-time dynamics of AB interferometers has been of recent interest, motivated by the challenge to understand quantum dynamics, particularly decoherence and dissipation, in open nonequilibrium quantum systems. Studies of electron dynamics in double-dot AB interferometers in the absence of e-e interactions have been carried out in Refs.<sup>17–19</sup>, using a non-markovian master equation approach. The role of e-e repulsion effects on the dots dynamics was studied numerically using a non-perturbative method in Ref.<sup>20</sup>.

In this paper, we focus on a simple-minimal model, the noninteracting double quantum dot AB interferometer, and study its transient and steady-state properties in biased situations. For a scheme of this model, see Fig. 1. This system has revealed a wealth of intricate behavior, such as “flux-dependent level attraction”<sup>21</sup>, and the ability to achieve decoherence control when junction asymmetry is incorporated<sup>19</sup>. Here, this noninteracting system further displays other non-trivial effects in both

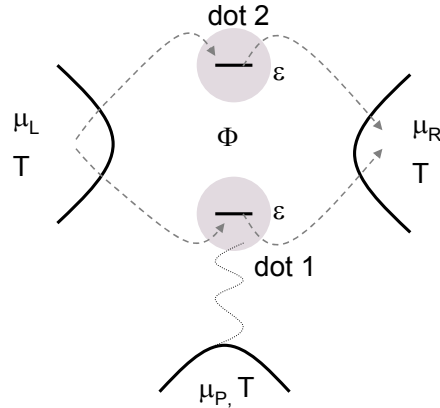


FIG. 1: Scheme of a double-dot AB interferometer. The two dots are each represented by a single electronic level, which do not directly couple. The total magnetic flux is denoted by  $\Phi$ . Dot ‘1’ may be susceptible to dephasing effects, introduced here through the coupling of this dot to a dephasing probe, the terminal  $P$ . The role of dephasing effects is discussed in Sec. V.

the transient regime and the stationary limit. While previous studies have allowed for junction asymmetry and nondegenerate dots<sup>18,21</sup>, we restrict ourselves to the simplest case of energy degenerate dots and symmetric dots-lead couplings. However, in our study the degenerate levels may be tuned *away* from the symmetric point, a situation that can be reached by applying a gating field. Using exact analytic expressions and numerical simulations, we expose several nontrivial effects emerging in this

biased-gated AB setup: (i) First, dots' occupations display strong flux dependency. (ii) Second, not only do the occupations vary with flux, but the dots acquire unequal occupations, at degeneracy. (iii) Further, we show that the effect of ‘‘phase localization’’<sup>17</sup> appears only at the symmetric point, while when the system is gated away from that point dot coherences can be feasibly controlled by the bias voltage.

In the stationary limit we further study the role of dephasing effects, implemented here through a dephasing probe<sup>22–24</sup>, on the coherence properties of the system. Interestingly, we find that finite and substantial dephasing strength, at the order of the bias voltage and dots energies, still allows for flux dependency of occupation. However, at finite dephasing the occupation-phase dependency significantly differs from the zero dephasing limit. In other words, finite dephasing alter coherent oscillations, to provide new features. The flux dependency of the occupation is fully washed out at a very strong dephasing strength.

The structure of the paper is as follows. In Sec. II we present the double-dot AB interferometer model. Sec. III explores the steady-state properties of the system using the nonequilibrium Green's function approach. We derive closed analytic expressions (at zero temperature) for the dots' level occupation, the coherence between the dots, and the charge current in the system. Sec. IV provides numerical results in the transient regime, indicating on the time scale it takes for the system to reach the stationary limit, and on the intricate dynamics involved. Sec. V. details the role of dephasing effects, providing analytic expressions for the dots occupations in the steady-state limit. Sec. VI summarizes our main results and concludes.

## II. MODEL

We focus on a symmetric AB setup, with a quantum dot located at each arm of the interferometer. The dots are connected to two metal leads (referred to as baths, or reservoirs) maintained in a biased state. For simplicity, we neglect the spin degree of freedom and describe each quantum dot by a spinless electronic level, see Fig. 1. The total Hamiltonian  $H$  includes the following terms

$$H = H_S + H_B + H_{SB}. \quad (1)$$

Here  $H_S$  is a subsystem (dots) Hamiltonian,  $H_B$  includes the two metals and  $H_{SB}$  incorporates subsystem-bath interaction terms. Specifically, we assume uncoupled dots,

$$H_S = \epsilon_1 a_1^\dagger a_1 + \epsilon_2 a_2^\dagger a_2. \quad (2)$$

To keep our discussion general, we allow the states to be nondegenerate at this point. In our analytic and numerical calculations below we have forced degeneracy.  $a_\beta^\dagger$  and  $a_\beta$  are the subsystem creation and annihilation operators,

respectively, where  $\beta = 1, 2$  denotes dots '1' and '2'. The metals are composed of noninteracting electrons,

$$H_B = \sum_l \omega_l a_l^\dagger a_l + \sum_r \omega_r a_r^\dagger a_r, \quad (3)$$

where  $a_{l,r}^\dagger$  and  $a_{l,r}$  are bath creation and annihilation operators, for the left ( $l \in L$ ) and right ( $r \in R$ ) leads. The subsystem-bath interaction term is given by

$$H_{SB} = \sum_{\beta,l} \xi_{\beta,l} a_\beta^\dagger a_l e^{i\phi_\beta^L} + \sum_{\beta,r} \zeta_{\beta,r} a_r^\dagger a_\beta e^{i\phi_\beta^R} + h.c., \quad (4)$$

where  $\xi$  is the coupling strength to left bath and similarly  $\zeta$  stands for the coupling strength to the right bath. The notation here is general, but we later take these couplings to be identical, since we are interested in a dot-lead symmetric setup. Here  $\phi_\beta^L$  and  $\phi_\beta^R$  are the AB phase factors, acquired by electron waves in a magnetic field perpendicular to the device plane. These phases are constrained to satisfy the following relation

$$\phi_1^L - \phi_2^L + \phi_1^R - \phi_2^R = \phi = 2\pi\Phi/\Phi_0. \quad (5)$$

$\Phi$  is the magnetic flux enclosed by the ring and  $\Phi_0 = hc/e$  is the flux quantum. In what follows we adopt the gauge  $\phi_1^L - \phi_2^L = \phi_1^R - \phi_2^R = \phi/2$ .

We voltage-bias the system, using the convention  $\Delta\mu \equiv \mu_L - \mu_R \geq 0$ , with  $\mu_{L,R}$  as the chemical potential of the metals. While we bias the system in a symmetric manner,  $\mu_L = -\mu_R$ , the dots levels may be placed away from the so called ‘‘symmetric point’’ at which  $\mu_L - \epsilon_\beta = \epsilon_\beta - \mu_R$ . This situation may be achieved by applying a gate voltage to each dot. For simplicity, we use the following conventions below,  $\hbar \equiv 1$  and electron charge  $e \equiv 1$ .

## III. STATIONARY BEHAVIOR

### A. Method: equations of motion

Since the model is noninteracting, its steady-state characteristics can be calculated exactly using the nonequilibrium Green's function (NEGF) approach<sup>25</sup>. This technique has been extensively used in the past for studying transport properties in mesoscopic systems and molecular junctions<sup>26</sup>. We review here the steps involved so as to carefully contain the phase factors. The derivation presented here follows an equation-of-motion approach<sup>27</sup>. In this method, an effective quantum Langevin equation for the subsystem is obtained by solving the Heisenberg equations of motion (EOM) for the baths variables, then substituting them back into the EOM for the subsystem (dots) variables. The indices

$\alpha, \beta = 1, 2$  identify the two dots. The resulting EOM is

$$\begin{aligned} \frac{da_\beta}{dt} &= -i\epsilon_\beta a_\beta - i\eta_\beta^L - i\eta_\beta^R \\ &- i \int_{t_0}^t d\tau \sum_{\alpha,l} \xi_{\beta,l} g_l^+(t-\tau) \xi_{\alpha,l}^* e^{i(\phi_\beta^L - \phi_\alpha^L)} a_\alpha(\tau) \\ &- i \int_{t_0}^t d\tau \sum_{\alpha,r} \zeta_{\beta,r}^* g_r^+(t-\tau) \zeta_{\alpha,r} e^{i(\phi_\alpha^R - \phi_\beta^R)} a_\alpha(\tau). \end{aligned} \quad (6)$$

The (isolated) reservoirs Green's functions are given by

$$g_l^+(t) = -ie^{-i\omega_l t} \theta(t), \quad g_r^+(t) = -ie^{-i\omega_r t} \theta(t). \quad (7)$$

The terms  $\eta_\beta^L$  and  $\eta_\beta^R$  are referred to as *noise*, induced on the subsystem from the left and right reservoirs, respectively. Their explicit form is

$$\begin{aligned} \eta_\beta^L &= i \sum_l \xi_{\beta,l} g_l^+(t-t_0) a_l(t_0) e^{i\phi_\beta^L} \\ \eta_\beta^R &= i \sum_r \zeta_{\beta,r}^* g_r^+(t-t_0) a_r(t_0) e^{-i\phi_\beta^R}. \end{aligned} \quad (8)$$

As an initial condition, we take a factorized state,  $\rho(t_0) = \rho_L \otimes \rho_R \otimes \rho_S(t_0)$ , with empty dots and the reservoirs prepared in a grand canonical state,  $\rho_\nu = \frac{e^{-(H_\nu - \mu_\nu N)/T_\nu}}{\text{Tr}[\rho_\nu]}$ ,  $T_\nu$  is the temperature of the  $\nu = L, R$  fermi sea and  $\mu_\nu$  stands for its chemical potential. The reduced density matrix  $\rho_S$  denotes the state of the subsystem. Using this initial condition, noise correlations satisfy

$$\begin{aligned} \langle \eta_\beta^{L\dagger}(t) \eta_{\beta'}^L(\tau) \rangle &= \sum_l \xi_{\beta,l}^* e^{i\omega_l(t-\tau)} \xi_{\beta',l} e^{-i(\phi_\beta^L - \phi_{\beta'}^L)} f_L(\omega_l) \\ \langle \eta_\beta^{R\dagger}(t) \eta_{\beta'}^R(\tau) \rangle &= \sum_r \zeta_{\beta,r} e^{i\omega_r(t-\tau)} \zeta_{\beta',r}^* e^{i(\phi_\beta^R - \phi_{\beta'}^R)} f_R(\omega_r), \end{aligned}$$

with the Fermi function  $f_\nu(\omega) = [e^{(\omega - \mu_\nu)/T_\nu} + 1]^{-1}$  and expectation values evaluated in the Heisenberg representation,  $\langle A(t) \rangle = \text{Tr}[\rho(t_0) A(t)]$ . Steady-state properties are reached by taking the limits  $t_0 \rightarrow -\infty$  and  $t \rightarrow \infty$ . We now Fourier transform Eq. (6) using the convolution theorem with the convention  $\tilde{a}_\beta(\omega) = \int_{-\infty}^{\infty} dt a_\beta(t) e^{i\omega t}$ ,  $\tilde{\eta}_\beta(\omega) = \int_{-\infty}^{\infty} dt \eta_\beta(t) e^{i\omega t}$ . The result, organized in a matrix form, is

$$\tilde{a}_\beta(\omega) = \sum_\alpha G_{\beta,\alpha}^+ [\tilde{\eta}_\alpha^L(\omega) + \tilde{\eta}_\alpha^R(\omega)], \quad (9)$$

with the Green's function

$$G_{\beta,\alpha}^+(\omega) = \frac{1}{(\omega - \epsilon_\beta) \delta_{\alpha,\beta} - \Sigma_{\beta,\alpha}^{L,+}(\omega) - \Sigma_{\beta,\alpha}^{R,+}(\omega)}. \quad (10)$$

The self energies contain the phase factors,

$$\begin{aligned} \Sigma_{\beta,\alpha}^{L,+}(\omega) &= \sum_l \xi_{\beta,l} g_l^+(\omega) \xi_{\alpha,l}^* e^{i(\phi_\beta^L - \phi_\alpha^L)}, \\ \Sigma_{\beta,\alpha}^{R,+}(\omega) &= \sum_r \zeta_{\beta,r}^* g_r^+(\omega) \zeta_{\alpha,r} e^{i(\phi_\alpha^R - \phi_\beta^R)}. \end{aligned} \quad (11)$$

We also define the conjugated-transposed matrix,  $G^- = (G^+)^\dagger$ , to be used below. The real part of the self energy is a principal value integral, assumed here to vanish. This assumption holds when the metals density of states is energy independent and the bandwidth is large. We then define the hybridization matrix from the relation  $\Sigma^+ = -i\Gamma/2$ ,

$$\Gamma_{\beta,\beta'}^L(\omega) = 2\pi e^{i(\phi_\beta^L - \phi_{\beta'}^L)} \sum_l \xi_{\beta,l} \delta(\omega - \omega_l) \xi_{\beta',l}^*. \quad (12)$$

Similar expressions hold for the  $R$  side. Using the steady-state solution (9), we can write down an expression for the reduced density matrix. Back transformed to the time domain it takes the form

$$\begin{aligned} \langle a_\alpha^\dagger a_\beta \rangle &\equiv \rho_{\alpha,\beta} = \frac{1}{2\pi} \int_{-\infty}^{\infty} \left[ (G^+ \Gamma^L G^-)_{\alpha,\beta} f_L(\omega) \right. \\ &\quad \left. + (G^+ \Gamma^R G^-)_{\alpha,\beta} f_R(\omega) \right] d\omega. \end{aligned} \quad (13)$$

The time variable has been suppressed since the result is only valid in the steady-state limit. In what follows we take  $\xi_{\beta,l}$  and  $\zeta_{\beta,r}$  as real constants, independent of the level index and the reservoir state, resulting in

$$\Gamma_{\beta,\beta'}^L = \gamma_L e^{i(\phi_\beta^L - \phi_{\beta'}^L)}, \quad \Gamma_{\beta,\beta'}^R = \gamma_R e^{-i(\phi_\beta^R - \phi_{\beta'}^R)}, \quad (14)$$

where the coefficient  $\gamma_\nu$ , defined through this relation and Eq. (12), is taken as a constant, energy independent. Using these definitions, the matrix  $G^+$  takes the form

$$G^+ = \begin{bmatrix} \omega - \epsilon_1 + \frac{i(\gamma_L + \gamma_R)}{2} & \frac{i\gamma_L}{2} e^{i\phi/2} + \frac{i\gamma_R}{2} e^{-i\phi/2} \\ \frac{i\gamma_L}{2} e^{-i\phi/2} + \frac{i\gamma_R}{2} e^{i\phi/2} & \omega - \epsilon_2 + \frac{i(\gamma_L + \gamma_R)}{2} \end{bmatrix}^{-1} \quad (15)$$

and the hybridization matrices are given by

$$\Gamma^L = \gamma_L \begin{bmatrix} 1 & e^{i\phi/2} \\ e^{-i\phi/2} & 1 \end{bmatrix}, \quad \Gamma^R = \gamma_R \begin{bmatrix} 1 & e^{-i\phi/2} \\ e^{i\phi/2} & 1 \end{bmatrix} \quad (16)$$

We can now calculate, numerically or analytically, the behavior of the reduced density matrix under different conditions<sup>18</sup>. Since we are only concerned here with *symmetric* dot-lead couplings, we take  $\gamma_L = \gamma_R = \gamma/2$ . Furthermore, we impose energy degeneracy,  $\epsilon_1 = \epsilon_2 = \epsilon$ . This choice simplifies the relevant matrices to

$$\begin{aligned} G^+ &= \left[ \begin{array}{cc} \omega - \epsilon + \frac{i\gamma}{2} & \frac{i\gamma}{2} \cos \frac{\phi}{2} \\ \frac{i\gamma}{2} \cos \frac{\phi}{2} & \omega - \epsilon + \frac{i\gamma}{2} \end{array} \right]^{-1}, \\ \Gamma^L &= \frac{\gamma}{2} \begin{bmatrix} 1 & e^{i\phi/2} \\ e^{-i\phi/2} & 1 \end{bmatrix}, \quad \Gamma^R = \frac{\gamma}{2} \begin{bmatrix} 1 & e^{-i\phi/2} \\ e^{i\phi/2} & 1 \end{bmatrix} \end{aligned} \quad (17)$$

We present closed analytic expressions for the diagonal and off-diagonal elements of the reduced density matrix in Sec. III.B. Complementing numerical data for the real-time dynamics are included in Sec. IV. This discussion is generalized in Sec. V, to include a dephasing probe.

## B. Observables

### 1. Dots occupation

We expose here two effects that persist away from the “symmetric point”, defined as  $\mu_L - \epsilon = \epsilon - \mu_R$ : The dots occupations significantly vary with flux, and moreover, the degenerate dots acquire different occupations. After presenting general expressions away from the symmetric point, we consider other relevant cases: the finite-bias limit at the symmetric point, the limit of infinite bias (which effectively reduces to the symmetric point), and the case of  $\phi = 2\pi n$ ,  $n = 0, 1, 2, \dots$

Analytic results are obtained from Eqs. (13) and (17). Organizing these expressions, we find that the occupation of dot '1',  $\rho_{1,1} \equiv \langle a_1^\dagger a_1 \rangle$ , is given by two integrals,

$$\rho_{1,1} = \frac{\gamma}{4\pi} \int_{-\infty}^{\infty} f_L(\omega) d\omega \frac{(\omega - \epsilon)^2 + \omega_0^2 - 2\omega_0(\omega - \epsilon) \cos \frac{\phi}{2}}{[(\omega - \epsilon)^2 - \omega_0^2]^2 + [\gamma(\omega - \epsilon)]^2} + \frac{\gamma}{4\pi} \int_{-\infty}^{\infty} f_R(\omega) d\omega \frac{(\omega - \epsilon)^2 + \omega_0^2 + 2\omega_0(\omega - \epsilon) \cos \frac{\phi}{2}}{[(\omega - \epsilon)^2 - \omega_0^2]^2 + [\gamma(\omega - \epsilon)]^2}, \quad (18)$$

where we have introduced the short notation

$$\omega_0 \equiv \frac{\gamma}{2} \sin \frac{\phi}{2}. \quad (19)$$

Similarly, the occupation of level '2',  $\rho_{2,2} \equiv \langle a_2^\dagger a_2 \rangle$ , is given by

$$\rho_{2,2} = \frac{\gamma}{4\pi} \int_{-\infty}^{\infty} f_L(\omega) d\omega \frac{(\omega - \epsilon)^2 + \omega_0^2 + 2\omega_0(\omega - \epsilon) \cos \frac{\phi}{2}}{[(\omega - \epsilon)^2 - \omega_0^2]^2 + [\gamma(\omega - \epsilon)]^2} + \frac{\gamma}{4\pi} \int_{-\infty}^{\infty} f_R(\omega) d\omega \frac{(\omega - \epsilon)^2 + \omega_0^2 - 2\omega_0(\omega - \epsilon) \cos \frac{\phi}{2}}{[(\omega - \epsilon)^2 - \omega_0^2]^2 + [\gamma(\omega - \epsilon)]^2}. \quad (20)$$

In what follows we consider the zero temperature limit. The Fermi functions take then the shape of step functions and the upper limits of the integrals are replaced by the corresponding chemical potentials. We now study the contribution of the odd term in the integrand. This term is responsible for the development of occupation difference between the dots,

$$\frac{\gamma}{4\pi} \int_{\mu_R}^{\mu_L} d\omega \frac{2\omega_0(\omega - \epsilon) \cos \frac{\phi}{2}}{[(\omega - \epsilon)^2 - \omega_0^2]^2 + [\gamma(\omega - \epsilon)]^2} = \frac{\sin \frac{\phi}{2}}{8\pi} \ln \left[ \frac{F_+(\phi)}{F_-(\phi)} \right], \quad (21)$$

where the explicit form of the factors  $F_{\pm}$  is

$$F_{\pm}(\phi) = \frac{\gamma^4}{8} \sin^4 \frac{\phi}{2} + 2(\mu_L - \epsilon)^2 (\mu_R - \epsilon)^2 + \frac{\gamma^2}{2} \left( \cos \frac{\phi}{2} \pm 1 \right)^2 (\mu_L - \epsilon)^2 + \frac{\gamma^2}{2} \left( \cos \frac{\phi}{2} \mp 1 \right)^2 (\mu_R - \epsilon)^2. \quad (22)$$

For details, see Appendix A. Since it is a sum of real quadratic terms,  $F_{\pm} \geq 0$ . Inspecting Eq. (21), we note that it vanishes in four different cases: (i) at zero bias, when  $\mu_L = \mu_R = 0$ , (ii) at infinite bias,  $\mu_L \rightarrow \infty$  and  $\mu_R \rightarrow -\infty$ , (iii) at the symmetric point when  $\mu_L - \epsilon = \epsilon - \mu_R$ , particularly for  $\epsilon = 0$  and  $\mu_L = -\mu_R$ , or when (iv)  $\phi = n\pi$ ,  $n = 0, 1, 2, \dots$  (leading to  $F_+ = F_-$ ). Combining Eq. (21) with the integration of even terms in Eq. (18), at zero temperature, we resolve the occupations

$$\rho_{1,1/2,2} = \frac{1}{4\pi} \left[ 2\pi + \tan^{-1} \left( \frac{\mu_L - \epsilon}{\gamma_-} \right) + \tan^{-1} \left( \frac{\mu_L - \epsilon}{\gamma_+} \right) + \tan^{-1} \left( \frac{\mu_R - \epsilon}{\gamma_-} \right) + \tan^{-1} \left( \frac{\mu_R - \epsilon}{\gamma_+} \right) \right] \pm \frac{\sin \frac{\phi}{2}}{8\pi} \ln \left[ \frac{F_-(\phi)}{F_+(\phi)} \right]. \quad (23)$$

The positive sign corresponds to  $\rho_{1,1}$ , the negative sign provides  $\rho_{2,2}$ . We have also introduced the short notation  $\gamma_{\pm} \equiv \frac{\gamma}{2}(1 \pm \cos \frac{\phi}{2})$ . Equation (23) predicts flux dependency of electron occupation *at degeneracy*, using symmetric hybridization constants, once the dots are tuned *away* from the symmetric point. Fig. 2 displays this behavior, and we find that as the dots energies get closer to the bias edge,  $\epsilon \sim \mu_L$ , the population strongly varies with  $\epsilon$  (panel b). It is also interesting to note that the abrupt jump at  $\phi = 2\pi n$  (discussed below) disappears once the levels reside at or above the bias window, for  $\epsilon \geq \mu_L$ . This feature results from the strict zero temperature limit assumed in the analytic calculations. At finite  $T$  the jump at  $\phi = 2\pi n$  survives even for  $\epsilon > \mu_L$ . However, when the temperature is at the order of the hybridization strength,  $T \sim \gamma$ , the modulation of the population with phase is washed out. The following parameters are used here and below: flat wide bands, dots energies at the order of  $\epsilon = 0 - 0.4$ , hybridization strength  $\gamma = 0.05 - 0.5$ , and a zero temperature, unless otherwise specified. The bias voltage is set symmetrically around the equilibrium Fermi energy,  $\mu_L = -\mu_R$ ,  $\Delta\mu \equiv \mu_L - \mu_R$ .

We now discuss in more details the behavior of the occupation in some special cases. First, we consider the symmetric point at finite bias and  $\phi \neq 2\pi n$ ,  $n = 0, 1, 2, \dots$ . In this case Eq. (23) precisely reduces to

$$\rho_{\alpha,\alpha}(\mu_L - \epsilon = \epsilon - \mu_R) = \frac{1}{2}. \quad (24)$$

This result holds in the infinite bias limit,  $\mu_L \rightarrow \infty$  and  $\mu_R \rightarrow -\infty$ , irrespective of the (finite) value of  $\epsilon$ . Next, the special case  $\phi = 2\pi n$  should be separately evaluated. At these points we have  $\omega_0 = 0$  and Eq. (18) provides the simple form at zero temperature

$$\rho_{\alpha,\alpha}(\phi = 2\pi n) = \frac{\gamma}{4\pi} \int_{-\infty}^{\mu_L - \epsilon} \frac{dx}{x^2 + \gamma^2} + \frac{\gamma}{4\pi} \int_{\epsilon - \mu_R}^{\infty} \frac{dx}{x^2 + \gamma^2} = \frac{1}{4\pi} \left[ \tan^{-1} \left( \frac{\mu_L - \epsilon}{\gamma} \right) + \tan^{-1} \left( \frac{\mu_R - \epsilon}{\gamma} \right) \right] + \frac{1}{4}. \quad (25)$$

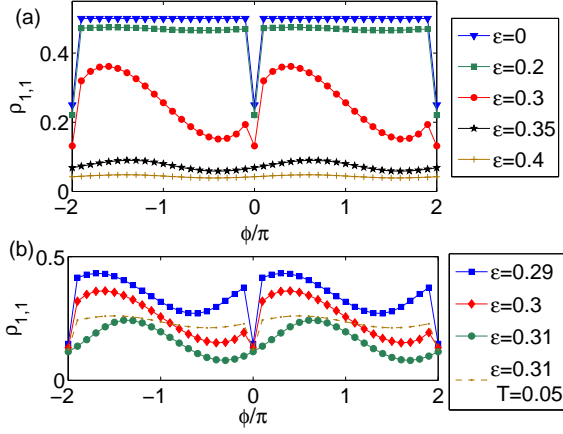


FIG. 2: (a) Flux dependency of occupation for dot '1' using  $\epsilon = 0$  (triangle),  $\epsilon = 0.2$  ( $\square$ ),  $\epsilon = 0.3$  ( $\circ$ ),  $\epsilon = 0.35$  ( $\star$ ) and  $\epsilon = 0.4$  ( $+$ ). Panel (b) displays results when  $\epsilon$  is tuned to the bias window edge,  $\epsilon \sim \mu_L$ ,  $\epsilon = 0.29$  ( $\square$ ),  $\epsilon = 0.3$  (diagonal),  $\epsilon = 0.31$  ( $\circ$ ), and  $\epsilon = 0.31$ ,  $T = 0.05$  (dashed-dotted line). In all cases  $\mu_L = -\mu_R = 0.3$ ,  $\gamma = 0.05$ , and  $T = 0$ , unless otherwise stated.

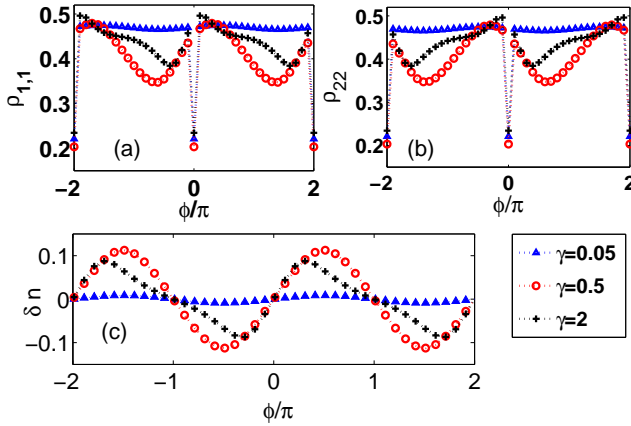


FIG. 3: (a)-(b) Dots occupations as a function of magnetic phase  $\phi$  for  $\Delta\mu = 0.6$ ,  $\epsilon = 0.2$ ,  $T = 0$ . (c) Occupation difference,  $\delta n = \rho_{1,1} - \rho_{2,2}$ . At weak coupling,  $\gamma = 0.05$  ( $\triangle$ ), the dots occupations are almost identical. When the hybridization is made stronger,  $\gamma = 0.5$  ( $\circ$ ), comparable to the levels displacement from the symmetric point,  $\rho_{1,1}$  clearly deviates from  $\rho_{2,2}$ . At very strong coupling,  $\gamma = 2$  ( $+$ ), the occupation difference reduces and asymmetries develop. For clarity, results are shown for  $\phi/\pi$  between  $(-2,2)$ .

These points are reflected by abrupt jumps in the occupations-flux behavior. Specifically, at the symmetric point there is a sharp reduction of occupation number from  $1/2$  [Eq. (24)] to  $1/4$  [Eq. (25)], as observed earlier in Ref.<sup>17</sup>. Fig. 2 shows that at strictly zero temperature this jump disappears once the dots energies are placed at or above the bias edge,  $\epsilon \geq \mu_L$ . Thus, the appearance of the jump is indicative of the fact that electrons cross the junction resonantly. If only tunneling processes contribute (once the dots' energies are placed above the bias

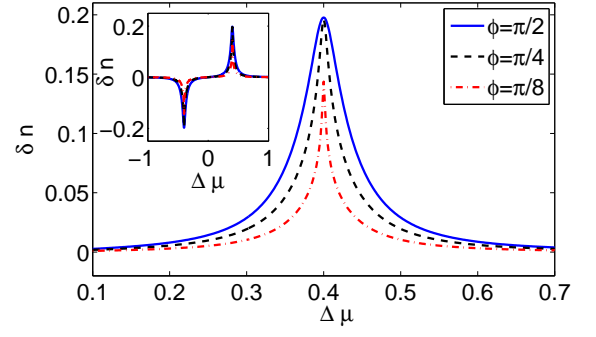


FIG. 4: Occupation difference as a function of bias voltage  $\Delta\mu$ , for different magnetic flux values,  $\phi = \pi/2$  (full line),  $\phi = \pi/4$  (dashed line),  $\phi = \pi/8$  (dashed-dotted line). Other parameters are  $\epsilon = 0.2$  and  $\gamma = 0.05$ ,  $T = 0$ . The inset presents data for backward and forward biases; the main plot zooms on the positive bias regime.

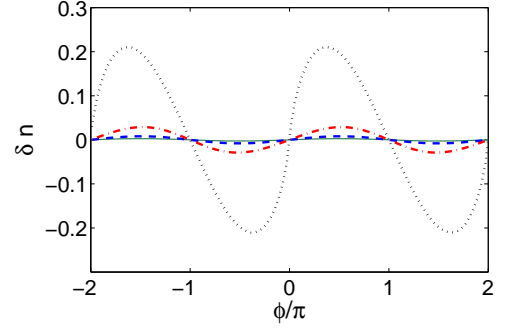


FIG. 5: Occupation difference as a function of magnetic flux for different bias values,  $\Delta\mu = 0.1$  (full line),  $\Delta\mu = 0.2$  (dashed line),  $\Delta\mu = 0.3$  (dashed-dotted line) and  $\Delta\mu = 0.4$  (dotted line). Other parameters are  $\epsilon = 0.2$ ,  $\gamma = 0.05$  and  $T = 0$ .

window and the temperature is very low), the population continuously vary with flux.

The total electronic occupation of the dots, at steady-state, generalizes the standard symmetric case attained in Ref.<sup>18</sup>,

$$\rho_{1,1} + \rho_{2,2} = \frac{\gamma}{2\pi} \int_{-\infty}^{\infty} d\omega \frac{[(\omega - \epsilon)^2 + \omega_0^2] [f_L(\omega) + f_R(\omega)]}{[(\omega - \epsilon)^2 - \omega_0^2]^2 + [\gamma(\omega - \epsilon)]^2}. \quad (26)$$

We now highlight one of the main results of the paper, the onset of occupation difference in this degenerate ( $\epsilon_1 = \epsilon_2$ ) and spatially symmetric ( $\gamma_L = \gamma_R$ ) setup. Using Eq. (23), we find that

$$\delta n \equiv \rho_{1,1} - \rho_{2,2} = \frac{\sin \frac{\phi}{2}}{4\pi} \ln \left[ \frac{F_-(\phi)}{F_+(\phi)} \right]. \quad (27)$$

As we mentioned above, this quantity is nonzero when the following (sufficient) conditions are simultaneously satisfied: (i) the bias voltage is finite, neither zero nor

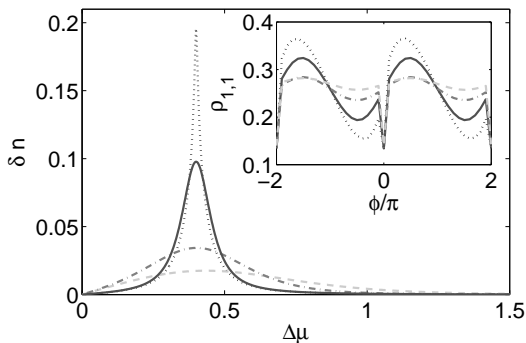


FIG. 6: Finite temperature effect. Main plot: Occupation difference as a function of bias voltage for  $\phi = \pi/4$ . Inset: occupation of dot '1' as a function of magnetic phase for  $\Delta\mu = 0.4$ . In both panels  $T = 0$  (dotted line),  $T = 0.01$  (full line),  $T = 0.05$  (dashed-dotted line) and  $T = 0.1$  (dashed line). Dots parameters are  $\epsilon = 0.2$  and  $\gamma = 0.05$ .

infinite, (ii) the dots are positioned away from the symmetric point,  $\epsilon \neq (\mu_L + \mu_R)/2$ , and (ii) the phase  $\phi$  is not a multiple of  $\pi$ ,  $\phi \neq n\pi$ ,  $n = 0, 1, 2, \dots$ . To rephrase this observation, the occupation difference can be controlled by manipulating the subsystem-metal hybridization energy  $\gamma$ , by changing the bias voltage, by applying a gate voltage for tuning the dots energies, and by modulating the phase  $\phi$  through the magnetic flux. The role of these control knobs are illustrated in Figures 3, 4 and 5.

In Fig. 3 we display the levels occupation in the resonant regime,  $\mu_R < \epsilon < \mu_L$  while varying  $\gamma$ . At weak coupling  $\delta n$  is insignificant. However, the occupation difference becomes large when co-tunneling effects contribute. More notably, Fig. 4 illustrates the strong controllability of  $\delta n$  with applied voltage. We find that the occupation difference is maximized at the edge of the resonant transmission window, when  $\mu_L - \epsilon = 0$  (or equivalently, when  $\Delta\mu = 2\epsilon$ ). The magnetic phase affects the width and height of the peak, but not the absolute position which

is only determined by the offset of  $\epsilon$  from the center of the bias window. In Fig. 5 we further show the flux dependency of  $\delta n$ , which is particularly significant when  $\Delta\mu = 2\epsilon$ .

The effect of finite temperature on the occupation-flux dependence, and on the development of occupation difference, is displayed in Fig. 6. We find that the effects largely survive at finite  $T$ , as long as  $T < \gamma$ . These results were calculated numerically, based on Eqs. (18) and (20).

## 2. Coherence

It was recently argued that the decoherence behavior in our generic setup, including two noninteracting (uncoupled) quantum dots interferometer, can be suppressed when the device geometry is made asymmetric and nondegenerate, using  $\epsilon_1 \neq \epsilon_2$  and  $\gamma_L \neq \gamma_R$ <sup>19</sup>. The requirement for asymmetry in this work arises from the observation of the ‘‘phase localization’’ effect, which hinders phase manipulation in the system at the symmetric point. The term ‘‘phase localization’’ refers to the fact that if we define  $\rho_{1,2}(t) = |\rho_{1,2}(t)|e^{i\varphi(t)}$ , the relative phase  $\varphi$  localizes to the values  $-\pi/2$  or  $\pi/2$  in the long time limit when  $\phi \neq 2\pi n$ ,  $n$  is an integer<sup>17</sup>. Based on numerical simulations, we have pointed out in Ref.<sup>20</sup> that phase localization occurs *only* at the symmetric point, while at other values of  $\epsilon$  the real part of  $\rho_{1,2}$  is finite and nonzero in the asymptotic limit for any phase besides  $2\pi n$ <sup>20</sup>. This observation is established here analytically in the steady-state limit, implying that decoherence could be suppressed in degenerate-symmetric systems by gating the dots, shifting their energies relative to the bias window.

We derive a closed expression for the off-diagonal system element  $\rho_{1,2} \equiv \langle a_1^\dagger a_2 \rangle$  by studying Eq. (13),

$$\rho_{12} = \frac{\gamma}{4\pi} \int_{-\infty}^{\infty} f_L(\omega) d\omega \left\{ \frac{\cos \frac{\phi}{2} [(\omega - \epsilon)^2 - \omega_0^2] + i \sin \frac{\phi}{2} [(\omega - \epsilon)^2 + \omega_0^2]}{[(\omega - \epsilon)^2 - \omega_0^2]^2 + [\gamma(\omega - \epsilon)]^2} \right\} + \frac{\gamma}{4\pi} \int_{-\infty}^{\infty} f_R(\omega) d\omega \left\{ \frac{\cos \frac{\phi}{2} [(\omega - \epsilon)^2 - \omega_0^2] - i \sin \frac{\phi}{2} [(\omega - \epsilon)^2 + \omega_0^2]}{[(\omega - \epsilon)^2 - \omega_0^2]^2 + [\gamma(\omega - \epsilon)]^2} \right\}. \quad (28)$$

At finite bias and zero temperature direct integration provides the real ( $\Re$ ) and imaginary ( $\Im$ ) parts of  $\rho_{1,2}$  ( $\phi \neq 2\pi n$ )

$$\Re \rho_{1,2} = \frac{1}{4\pi} \left[ \tan^{-1} \left( \frac{\mu_L - \epsilon}{\gamma_+} \right) - \tan^{-1} \left( \frac{\mu_L - \epsilon}{\gamma_-} \right) + \tan^{-1} \left( \frac{\mu_R - \epsilon}{\gamma_+} \right) - \tan^{-1} \left( \frac{\mu_R - \epsilon}{\gamma_-} \right) \right], \quad (29)$$

and

$$\Im \rho_{1,2} = \frac{1}{4\pi} \sin(\phi/2) \left[ \tan^{-1} \left( \frac{\mu_L - \epsilon}{\gamma_+} \right) + \tan^{-1} \left( \frac{\mu_L - \epsilon}{\gamma_-} \right) - \tan^{-1} \left( \frac{\mu_R - \epsilon}{\gamma_+} \right) - \tan^{-1} \left( \frac{\mu_R - \epsilon}{\gamma_-} \right) \right]. \quad (30)$$

As before, we define  $\gamma_{\pm} = \frac{\gamma}{2}(1 \pm \cos \frac{\phi}{2})$ . We now readily

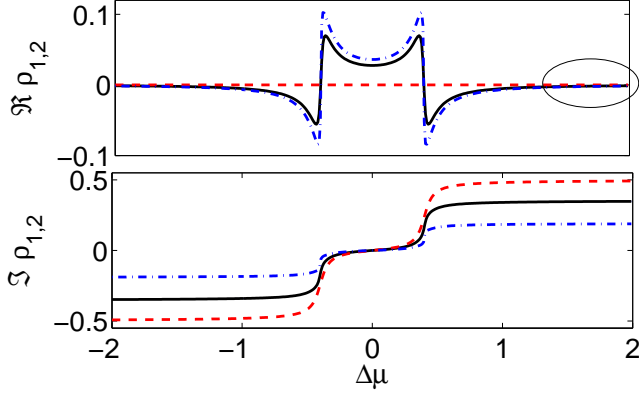


FIG. 7: Real and imaginary parts of the coherence as a function of the bias voltage.  $\phi = \pi$  (dashed line),  $\phi = \pi/2$  (full line),  $\phi = \pi/4$  (dashed-dotted line). Other parameters are  $\epsilon = 0.2$ ,  $\gamma = 0.05$ , and  $T = 0$ . The oval shape marks the region of phase localization at positive bias.

confirm that at the symmetric point the real part vanishes and “phase localization” takes place<sup>17</sup>. In particular, in the infinite bias limit we find  $\Re \rho_{1,2} = \frac{1}{2} \sin \frac{\phi}{2}$ , in agreement with previous studies<sup>20</sup>. We also include the behavior at the special points  $\phi = 2\pi n$ . Eq. (28) reduces then to a simple Lorentzian form, at zero temperature,

$$\begin{aligned} \rho_{1,2}(\phi = 0) &= \frac{\gamma}{4\pi} \int_{-\infty}^{\mu_L - \epsilon} \frac{dx}{x^2 + \gamma^2} + \frac{\gamma}{4\pi} \int_{\epsilon - \mu_R}^{\infty} \frac{dx}{x^2 + \gamma^2} \\ &= \frac{1}{4\pi} \left[ \tan^{-1} \left( \frac{\mu_L - \epsilon}{\gamma} \right) + \tan^{-1} \left( \frac{\mu_R - \epsilon}{\gamma} \right) \right] + \frac{1}{4}. \end{aligned} \quad (31)$$

The sign reverses for  $\phi = \pm 2\pi$ . We note that the imaginary part of the coherence identically vanishes at zero phase while the real part is finite, approaching the value  $1/4$  at the symmetric point.

Numerical results in the steady-state limit are displayed in Fig. 7. We find that both the real and imaginary parts of  $\rho_{1,2}$  demonstrate significant features when the dots’ levels cross the bias window, at  $\Delta\mu = 2\epsilon$ . The value of the real part abruptly changes sign, the imaginary part develops a step. At large bias  $\Re \rho_{1,2}$  diminishes while  $\Im \rho_{1,2}$  is finite, indicating on the development of the phase localization behavior. It can be shown that the double-step structure of  $\Im \rho_{1,2}$  (as a function of  $\Delta\mu$ ) disappears when the dots energies are set at the symmetric point.

### 3. Current

It is of interest to complement our study of subsystem (dots) properties and examine the transmission coefficient and the overall charge current in the system. The electric current, flowing from the  $L$  metal to the  $R$  end, is

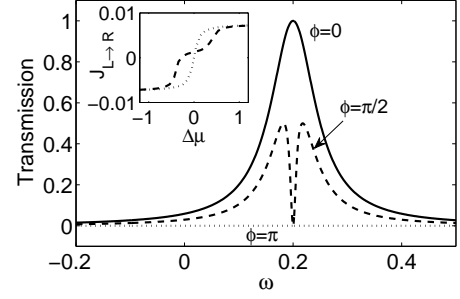


FIG. 8: Transmission coefficient as a function of energy for  $\epsilon = 0.2$ ,  $\gamma = 0.05$ ,  $\phi = \pi$  (dotted line),  $\phi = \pi/2$  (dashed line) and  $\phi = 0$  (full line). The inset presents the charge current for  $\phi = \pi/2$  and  $\epsilon = 0.2$  (dashed line),  $\epsilon = 0$  (dotted line).

obtained by defining the number operator  $N_L \equiv \sum_l a_l^\dagger a_l$ , providing the current  $J_{L \rightarrow R} = -\frac{dN_L}{dt} = -i[H, N_L]$ . This yields

$$J_{L \rightarrow R} = i \sum_{l,\alpha=1,2} \left( \xi_{\alpha,l}^* e^{-i\phi_\alpha^L} \langle a_l^\dagger a_\alpha \rangle - \xi_{\alpha,l} e^{i\phi_\alpha^L} \langle a_\alpha^\dagger a_l \rangle \right) \quad (32)$$

Expectation values are calculated in the steady-state limit. Using the EOM formalism as explained in Sec. III, we get the standard result<sup>25</sup>

$$J_{L \rightarrow R} = \frac{1}{2\pi} \int_{-\infty}^{\infty} d\omega \mathcal{T}_{LR}(\omega) [f_L(\omega) - f_R(\omega)]. \quad (33)$$

The transmission coefficient is defined as  $\mathcal{T}_{LR} = \text{Tr}(\Gamma^L G^+ \Gamma^R G^-)$ , where the trace is performed over the states of the subsystem (dots). In the present model, at zero temperature, we obtain

$$\begin{aligned} J_{L \rightarrow R} &= \frac{1}{2\pi} \int_{\mu_L}^{\mu_R} d\omega \frac{\gamma^2 (\omega - \epsilon)^2 \cos^2 \frac{\phi}{2}}{[(\omega - \epsilon)^2 - \omega_0^2]^2 + \gamma^2 (\omega - \epsilon)^2} \\ &= \frac{\cos \frac{\phi}{2}}{2\pi} \left[ \gamma_+ \left\{ \tan^{-1} \left( \frac{\mu_L - \epsilon}{\gamma_+} \right) - \tan^{-1} \left( \frac{\mu_R - \epsilon}{\gamma_+} \right) \right\} \right. \\ &\quad \left. - \gamma_- \left\{ \tan^{-1} \left( \frac{\mu_L - \epsilon}{\gamma_-} \right) - \tan^{-1} \left( \frac{\mu_R - \epsilon}{\gamma_-} \right) \right\} \right], \end{aligned} \quad (34)$$

which agrees with known results<sup>5</sup>. Using the NEGF formalism, we could similarly investigate the shot noise in the double-dot AB interferometer<sup>28</sup>.

The transmission function is plotted in Fig. 8 displaying destructive interference pattern for  $\phi = \pi$  and a constructive behavior for  $\phi = 0$ . For  $\phi \neq n\pi$  the transmission nullifies exactly at the position of the resonant level<sup>29</sup>. The inset presents the current-voltage characteristics for  $\phi = \pi/2$  away from the symmetric point (dashed line), and at the symmetric point (dotted line). We note that the double-step structure disappears at the latter case. It can be shown that the double step structure of  $\Im \rho_{1,2}$  (see Fig. 7) similarly diminishes at the symmetric point.



#### IV. TRANSIENT BEHAVIOR

It is of interest to investigate the development of the phase dependency of the occupancy, and the occupancy difference  $\delta n$ , before steady-state sets. Similarly, the dynamics of coherences is nontrivial even without electron-electron interaction effects<sup>20</sup>. We complement the NEGF steady-state expressions of Sec. III with numerical calculations of the transient behavior using an exact numerical tool that is based on the fermionic trace formula<sup>30</sup>

$$\text{Tr} [e^{M_1} e^{M_2} \dots e^{M_p}] = \det [1 + e^{m_1} e^{m_2} \dots e^{m_p}]. \quad (35)$$

Here  $m_p$  is a single-particle operator corresponding to a quadratic operator  $M_p = \sum_{i,j} (m_p)_{i,j} a_i^\dagger a_j$ .  $a_i^\dagger$  ( $a_j$ ) are fermionic creation (annihilation) operators. The trace is performed over all electronic degrees of freedom. Our objective is the dynamics of a quadratic operator  $B \equiv a_j^\dagger a_k$ ,  $j, k = 1, 2$ ,

$$\begin{aligned} \langle B(t) \rangle &= \text{Tr} [\rho(t_0) e^{iHt} B e^{-iHt}] \\ &= \lim_{\lambda \rightarrow 0} \frac{\partial}{\partial \lambda} \text{Tr} [\rho_L \rho_R \rho_S e^{iHt} e^{\lambda B} e^{-iHt}]. \end{aligned} \quad (36)$$

We introduce the  $\lambda$  parameter, taken to vanish at the end of the calculation. The initial condition is factorized,  $\rho(t_0) = \rho_S \otimes \rho_L \otimes \rho_R$ , and these density operators follow an exponential form,  $e^M$ , with  $M$  a quadratic operator. The application of the trace formula leads to

$$\begin{aligned} \langle e^{\lambda B(t)} \rangle &= \det \left\{ [I_L - f_L] \otimes [I_R - f_R] \otimes [I_S - f_S] \right. \\ &\quad \left. + e^{iht} e^{\lambda b} e^{-iht} f_L \otimes f_R \otimes f_S \right\}. \end{aligned} \quad (37)$$

with  $b$  and  $h$  as the single-body matrices of the  $B$  and  $H$  operators, respectively. The matrices  $I_\nu$  and  $I_S$  are the identity matrices for the  $\nu = L, R$  space and for the subsystem (dots). The functions  $f_L$  and  $f_R$  are the band electrons occupancy  $f_\nu(\epsilon) = [e^{\beta(\epsilon - \mu_\nu)} + 1]^{-1}$ . Here they are written in matrix form and in the energy representation.  $f_S$  represents the initial occupation for the dots, assumed empty, again written in a matrix form. When working with finite-size reservoirs, Eq. (37) can be readily simulated numerically-exactly.

Fig. 9 displays the evolution of the occupation difference, presented as a function of  $\Delta\mu$ . In this simulation we used finite bands with a sharp cutoff,  $D = \pm 1$ . At short time  $\delta n$  shows weak sensitivity to the actual bias. Only after a certain time,  $\gamma t \sim 2$ , the peak around the edge at  $\Delta\mu = 2\epsilon$  clearly develops. Note that since the band is not very broad, edge effects are reflected at large biases as nonzero occupation difference, in contrast to the broad-bandwidth long-time behavior of Fig. 4.

The transient behavior of the coherences,  $\Re\rho_{1,2}$  and  $\Im\rho_{1,2}$ , is included in Fig. 10; the corresponding steady-state value are presented in Fig. 7. We can follow the temporal features of the phase localization effect, i.e., the disappearance of the real part of the coherence at the

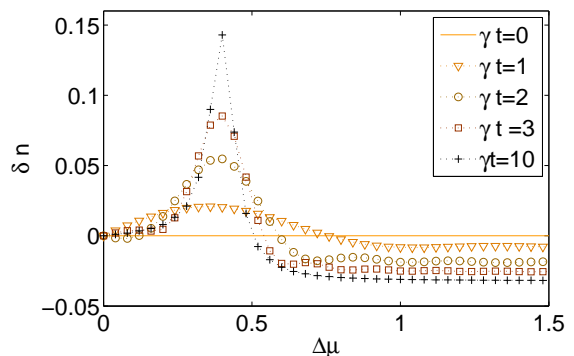


FIG. 9: Time evolution of the occupation difference,  $\gamma = 0.05$ ,  $\epsilon = 0.2$ ,  $T = 5 \times 10^{-3}$ ,  $\phi = \pi/2$ .

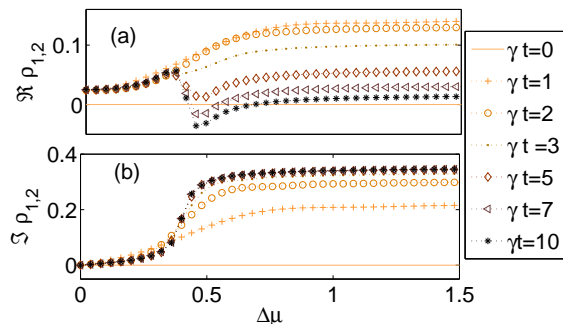


FIG. 10: Time evolution of the real (a) and imaginary (b) parts of the coherence  $\gamma = 0.05$ ,  $\epsilon = 0.2$ ,  $T = 5 \times 10^{-3}$ ,  $\phi = \pi/2$ .

symmetric point or at large bias, when  $\phi \neq 2\pi n$ . Using  $\phi = \pi/2$  we note that while at short to intermediate time ( $\gamma t < 2$ ) significant coherence builds up, the real part of the coherence eventually survives only at small biases. Regarding timescales, we find that while  $\Im\rho_{1,2}$  reaches the steady-state values at short time,  $\gamma t \sim 2$ ,  $\Re\rho_{1,2}$  approaches its stationary limit only at longer times, for  $\gamma t \sim 10$ . Similar results were obtained in Ref.<sup>20</sup>.

#### V. DEPHASING PROBE: STEADY STATE CHARACTERISTICS

We have discussed so far pure coherent evolution effects in double-dot AB interferometers. It is important to examine at this point the role of elastic dephasing effects on this evolution as was done experimentally<sup>33,34</sup> and theoretically<sup>35-37</sup> in related systems. Here, we are essentially focused on the effect of dephasing on the modulation of occupation with magnetic phase. Recently, interference and decoherence processes were studied not only in quantum dot structures<sup>23,24</sup>, but in molecular loops as well<sup>15,16,38,39</sup>.

Phase-breaking processes arise due to the interaction of electrons with other degrees of freedom, e.g., with elec-



trons, phonons and defects. We generalize here the discussion of Sec. III, and incorporate dephasing processes into our system phenomenologically, by using the well established method of Büttiker dephasing probe<sup>22</sup>. In this technique, elastic dephasing processes on the dots are emulated by including a third terminal,  $P$ , enforcing the requirement that the charge current towards the probe terminal, at a given electron energy, should vanish. Thus, electrons travel to the probe and return to the system with a different phase, while both electron number and electron energy are conserved. This condition sets an electron distribution within the probe. As we show below, away from the symmetric point this distribution effectively depends on the magnetic phase. Other phenomenological tools to incorporate dephasing processes in mesoscopic devices are based on the introduction of random-phase fluctuations into the scattering matrix<sup>31</sup>, or on the inclusion of damping terms into the off-diagonal elements of the density matrix within quantum master equations (Lindblad or Redfield) formalisms<sup>32</sup>.

Using Büttiker probe method, we augment the Hamiltonian (1) with a probe, adding to the system a noninteracting electron reservoir  $P$ ,

$$H_D = H + \sum_{p \in P} \omega_p a_p^\dagger a_p + \sum_{p \in P} \lambda_p a_1^\dagger a_p + h.c. \quad (38)$$

The parameter  $\lambda$  denotes the coupling strength of dot '1' to the  $P$  terminal, taken as a real number. Note that we only allow here for local dephasing on dot '1'. One could similarly consider models where both dots are susceptible to dephasing effects, possibly from different sources. Following the equations-of-motion approach as detailed in Sec. III, we arrive at the steady-state expression for the reduced density matrix

$$\langle a_\alpha^\dagger a_\beta \rangle = \frac{1}{2\pi} \sum_{\nu=L,R,P} \int_{-\infty}^{\infty} (G^+ \Gamma^\nu G^-)_{\alpha,\beta} f_\nu(\omega) d\omega. \quad (39)$$

The probe hybridization matrix is given by

$$\Gamma^P = \gamma_P \begin{bmatrix} 1 & 0 \\ 0 & 0 \end{bmatrix}, \quad (40)$$

and the dot's Green's function is written by generalizing the matrix (15), to include the probe self energy,

$$G^+ = \left[ \begin{array}{cc} \omega - \epsilon_1 + \frac{i(\gamma_L + \gamma_R + \gamma_P)}{2} & \frac{i\gamma_L}{2} e^{i\phi/2} + \frac{i\gamma_R}{2} e^{-i\phi/2} \\ \frac{i\gamma_L}{2} e^{-i\phi/2} + \frac{i\gamma_R}{2} e^{i\phi/2} & \omega - \epsilon_2 + \frac{i(\gamma_L + \gamma_R)}{2} \end{array} \right]^{-1}.$$

This matrix is written here in a general form, to allow one to distinguish between the two dots and the different dots-metals hybridization terms. The dot-probe hybridization is defined as  $\gamma_P = 2\pi \sum_p |\lambda_p|^2 \delta(\omega - \omega_0)$ , in analogy with Eq. (12). In our calculations below we assume energy degenerate dots and symmetric couplings,  $\epsilon = \epsilon_1 = \epsilon_2$ ,  $\gamma_L = \gamma_R = \gamma/2$ .

We now derive the probe distribution by demanding that the energy resolved charge current to the  $P$  terminal vanishes. The total current to  $P$  is given by the sum of the currents from the  $L$  and  $R$  terminals, generalizing Eq. (33),

$$\begin{aligned} J_P &= J_{L \rightarrow P} + J_{R \rightarrow P} \\ &= \frac{1}{2\pi} \int_{-\infty}^{\infty} \mathcal{T}_{LP}(\omega) [f_L(\omega) - f_P(\omega)] d\omega \\ &\quad + \frac{1}{2\pi} \int_{-\infty}^{\infty} \mathcal{T}_{RP}(\omega) [f_R(\omega) - f_P(\omega)] d\omega \end{aligned} \quad (41)$$

with the transmission coefficient  $\mathcal{T}_{\nu\bar{\nu}}(\omega) = \text{Tr}[\Gamma^\nu G^+ \Gamma^{\bar{\nu}} G^-]$ . By requiring the integrand to vanish, we arrive at the probe distribution

$$f_P(\omega) = \frac{\mathcal{T}_{LP}(\omega) f_L(\omega) + \mathcal{T}_{RP}(\omega) f_R(\omega)}{\mathcal{T}_{LP}(\omega) + \mathcal{T}_{RP}(\omega)}. \quad (42)$$

Direct evaluation of these transmission coefficients provide the electron distribution in the probe,

$$\begin{aligned} f_P(\omega) &= \frac{f_L(\omega) + f_R(\omega)}{2} \\ &\quad + \frac{\gamma(\omega - \epsilon) \sin \frac{\phi}{2} \cos \frac{\phi}{2}}{2[(\omega - \epsilon)^2 + \omega_0^2]} [f_L(\omega) - f_R(\omega)]. \end{aligned} \quad (43)$$

As before,  $\omega_0 = \frac{\gamma}{2} \sin \frac{\phi}{2}$ . This expression indicates that the magnetic flux plays a role in setting the distribution within the probe, (such that it only dephases the system and does not deplete electrons or allow energy reorganization). This dependency disappears when the dots energies are set at the symmetric point, since the contribution of the second term in Eq. (43) diminishes in the integrals of Eq. (44), from symmetry considerations. We now write integral expressions for the dots occupations using Eq. (39),

$$\begin{aligned}
\rho_{1,1} &= \frac{\gamma}{4\pi} \int_{-\infty}^{\infty} \frac{d\omega}{\Delta(\omega)} \left\{ \left[ (\omega - \epsilon)^2 + \omega_0^2 - 2\omega_0(\omega - \epsilon) \cos \frac{\phi}{2} \right] f_L(\omega) + \left[ (\omega - \epsilon)^2 + \omega_0^2 + 2\omega_0(\omega - \epsilon) \cos \frac{\phi}{2} \right] f_R(\omega) \right\} \\
&+ \frac{\gamma_P}{2\pi} \int_{-\infty}^{\infty} \frac{d\omega}{\Delta(\omega)} \left[ (\omega - \epsilon)^2 + \frac{\gamma^2}{4} \right] f_P(\omega) \\
\rho_{2,2} &= \frac{\gamma}{4\pi} \int_{-\infty}^{\infty} \frac{d\omega}{\Delta(\omega)} \left\{ \left[ (\omega - \epsilon)^2 + \omega_0^2 + 2\omega_0(\omega - \epsilon) \cos \frac{\phi}{2} + \omega_0 \gamma_P \sin \frac{\phi}{2} + \frac{\gamma_P^2}{4} \right] f_L(\omega) \right. \\
&+ \left. \left[ (\omega - \epsilon)^2 + \omega_0^2 - 2\omega_0(\omega - \epsilon) \cos \frac{\phi}{2} + \omega_0 \gamma_P \sin \frac{\phi}{2} + \frac{\gamma_P^2}{4} \right] f_R(\omega) \right\} \\
&+ \frac{\gamma^2 \gamma_P}{8\pi} \cos^2 \frac{\phi}{2} \int_{-\infty}^{\infty} \frac{d\omega}{\Delta(\omega)} f_P(\omega),
\end{aligned} \tag{44}$$

with

$$\Delta(\omega) = \left| (\omega - \epsilon)^2 - \omega_0^2 - \frac{\gamma \gamma_P}{4} + i \left( \gamma + \frac{\gamma_P}{2} \right) (\omega - \epsilon) \right|^2.$$

In the absence of dephasing these expressions reduce to Eqs. (18) and (20). In the opposite limit, at very large dephasing,  $\gamma_P \gg \gamma$ ,  $\gamma_P > \Delta\mu$ , we note that  $\rho_{2,2}$  is dominated by  $\gamma_P^2 \gamma$  terms that are flux independent, while  $\rho_{1,1}$  is dominated by its last term,  $\propto \gamma_P f_P$ , which is flux dependent away from the symmetric point, resulting in  $\rho_{1,1} \propto \sin(\phi)$ . Thus, quite counter-intuitively, we find that the level that is directly susceptible to local dephasing demonstrates flux dependency of occupation at strong dephasing, while the level that *indirectly* suffers dephasing effects more feasibly loses its coherent oscillations.

Using numerical integration, dots occupations and their oscillation with phase are presented in Fig. 11. We observe the following trends upon increasing dephasing strength: At the symmetric point, (a)-(b), the abrupt jump at zero magnetic phase immediately disappears with the application of finite dephasing. When the dot energies are placed away from the symmetric point, yet they buried within the bias window, (c)-(d), the abrupt jump at zero magnetic phase again disappears, though the oscillations of occupation with phase prevail till large dephasing,  $\gamma_P \sim \Delta\mu$ . More significantly, when the dots energies are tuned at the edge of the bias window, (e)-(f), we find that dot '1' (which is directly dephased) develops new type of oscillation with phase. Only at very large dephasing,  $\gamma_P \gg \Delta\mu$ , these oscillations are overly suppressed. Thus, away from the symmetric point not only features of coherent dynamics survive even at significant dephasing strength, new type of coherent oscillations may develop as a result of the application of elastic scattering effects on the dots. It is interesting to reproduce this behavior while modeling elastic dephasing effects using other techniques<sup>31,32,35-37</sup>.

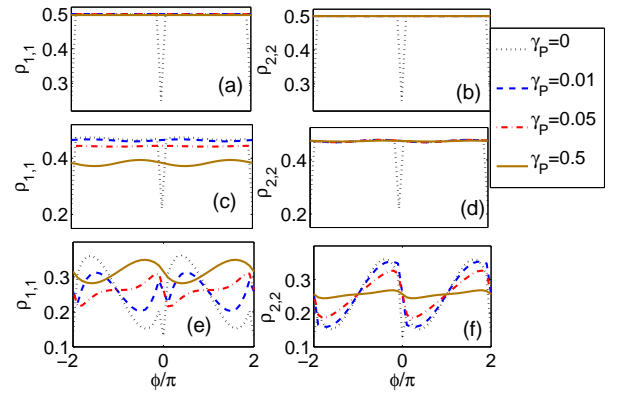


FIG. 11: The role of dephasing on the dots occupations - magnetic phase dependency, (a)-(b)  $\epsilon = 0$ , (c)-(d)  $\epsilon = 0.2$ , (e)-(f)  $\epsilon = 0.3$ , where  $\gamma_P=0$  (dotted line),  $\gamma_P = 0.01$  (dashed line),  $\gamma_P = 0.05$  (dashed-dotted line) and  $\gamma_P = 0.5$  (full line). Other parameters are  $\gamma = 0.05$ ,  $\Delta\mu = 0.6$ ,  $T = 0$ .

## VI. CONCLUSIONS

In this paper, we have addressed the issue of magnetic field control on electronic occupation and coherence in double-dot AB interferometers. The system under investigation included energy degenerate dots with symmetric dot-metals hybridization strengths. However, by voltage gating the dots energies away from the so-called symmetric point at which  $\epsilon = (\mu_L + \mu_R)/2$  we have resolved four nontrivial effects that can allow for significant controllability over dots occupations and their coherence: (i) Dots occupations may significantly vary with magnetic flux, particularly when the dots levels reside close to the bias edge. (ii) The dots acquire different occupations, though they are energy degenerate. This behavior is maximized at the bias edge  $\epsilon \sim \mu_L$ . It survives at finite temperature, as long as  $T < \gamma$ . (iii) Regarding the dots coherence, we have proven that the effect of “phase localization”<sup>17</sup> does not take place away from

the symmetric point, allowing for decoherence control in the system. Furthermore, (iv) we have found that away from the symmetric point the system can withstand dephasing processes, maintaining its coherent evolution and even develop new type of oscillations under intermediate dephasing strengths ( $\gamma_P \sim \Delta\mu$ , and  $\gamma_P \gg \gamma$ ).

Our minimal model could be applied to describe magnetic field control in mesoscopic conducting loops and in molecular ring structures. In the latter case it was particularly noted that degeneracy is crucial for allowing controllability within realistic magnetic fields<sup>15</sup>. Our study has been limited to the noninteracting electron model, excluding both electron-electron interaction effects and other explicit sources for dephasing and inelastic scattering processes. It is of interest to explore the role of interactions on the effects revealed in this paper, as we expect it to lift the energy degeneracy in the system, further intensifying the effects discussed here. This behavior can be immediately observed at the mean-field level. The Hartree term corrects the dots energies, e.g.  $\epsilon_1 \rightarrow \epsilon_1 + U\rho_{2,2}$ <sup>40</sup>. Thus, away from the symmetric point, (flux generated) unequal dots occupations translate to effective unequal energetics for the two (identical) dots.

### Acknowledgments

DS acknowledges support from NSERC discovery grant. The research of SB was supported by an Early Research Award of DS. The authors acknowledge Savannah Garmon for useful discussions.

### Appendix A: Derivation of Equation (21)

In this appendix our aim is to evaluate the following integral analytically

$$I = \frac{\gamma}{4\pi} \int_{\mu_R}^{\mu_L} d\omega \frac{2\omega_0(\omega - \epsilon) \cos \frac{\phi}{2}}{[(\omega - \epsilon)^2 - \omega_0^2]^2 + [\gamma(\omega - \epsilon)]^2}. \quad (\text{A1})$$

We achieve this by using the following definite integral

$$I_0 = \int_d^c \frac{x}{(x^2 - a^2)^2 + b^2 x^2} dx \\ = \frac{\tan^{-1} \left[ \frac{2a^2 - b^2 - 2d^2}{b\sqrt{4a^2 - b^2}} \right] - \tan^{-1} \left[ \frac{2a^2 - b^2 - 2c^2}{b\sqrt{4a^2 - b^2}} \right]}{b\sqrt{4a^2 - b^2}} \quad (\text{A2})$$

where  $d = (\mu_R - \epsilon)$ ,  $c = (\mu_L - \epsilon)$ ,  $b = \gamma$  and  $a = \frac{\gamma}{2} \sin \frac{\phi}{2}$ , leading to  $b\sqrt{4a^2 - b^2} = \pm i\gamma^2 \cos \frac{\phi}{2}$  and

$$2a^2 - b^2 - 2d^2 = \gamma^2 \left[ \frac{1}{2} \sin^2 \frac{\phi}{2} - 1 \right] - 2(\mu_R - \epsilon)^2$$

$$2a^2 - b^2 - 2c^2 = \gamma^2 \left[ \frac{1}{2} \sin^2 \frac{\phi}{2} - 1 \right] - 2(\mu_L - \epsilon)^2$$

We now reorganize Eq. (A2) using the relations  $\tan^{-1} x + \tan^{-1} y = \tan^{-1} \left( \frac{x+y}{1-xy} \right)$  and  $\tan^{-1} z = \frac{i}{2} [\ln(1 - iz) - \ln(1 + iz)]$ , to find

$$I_0 = \frac{\ln \left[ \frac{F_+(\phi)}{F_-(\phi)} \right]}{2\gamma^2 \cos \frac{\phi}{2}}, \quad (\text{A3})$$

where we define

$$F_{\pm}(\phi) = \frac{\gamma^4}{8} \sin^4 \frac{\phi}{2} \\ - (\mu_L - \epsilon)^2 \left[ \frac{\gamma^2}{2} \sin^2 \frac{\phi}{2} - (\mu_R - \epsilon)^2 - \gamma^2 \left( 1 \pm \cos \frac{\phi}{2} \right) \right] \\ - (\mu_R - \epsilon)^2 \left[ \frac{\gamma^2}{2} \sin^2 \frac{\phi}{2} - (\mu_L - \epsilon)^2 - \gamma^2 \left( 1 \mp \cos \frac{\phi}{2} \right) \right]. \quad (\text{A4})$$

We can also reorganize these factors as a sum of real quadratic terms,

$$F_{\pm}(\phi) = \frac{\gamma^4}{8} \sin^4 \frac{\phi}{2} + 2(\mu_L - \epsilon)^2 (\mu_R - \epsilon)^2 \\ + \frac{\gamma^2}{2} \left( \cos \frac{\phi}{2} \pm 1 \right)^2 (\mu_L - \epsilon)^2 \\ + \frac{\gamma^2}{2} \left( \cos \frac{\phi}{2} \mp 1 \right)^2 (\mu_R - \epsilon)^2. \quad (\text{A5})$$

Attaching the missing prefactors,  $I = \frac{\gamma}{4\pi} 2\omega_0 \cos \frac{\phi}{2} I_0$ , we obtain Eq. (21)

$$I = \frac{\sin \frac{\phi}{2}}{8\pi} \ln \left[ \frac{F_+(\phi)}{F_-(\phi)} \right]. \quad (\text{A6})$$

<sup>1</sup> G. Hackenbroich, Phys. Rep. **343**, 463 (2001), and references therein.

<sup>2</sup> Y. Imry, *Introduction to Mesoscopic Physics*, 2nd ed. (Oxford University Press, Oxford, 2002).

<sup>3</sup> A. Yacoby, M. Heiblum, D. Mahalu, and H. Shtrikman, Phys. Rev. Lett. **74**, 4047 (1995).

<sup>4</sup> R. Schuster, E. Buks, M. Heiblum, D. Mahalu, V. Umansky, and H. Shtrikman, Nature **385**, 417 (1997).

<sup>5</sup> J. König and Y. Gefen, Phys. Rev. Lett. **86**, 3855 (2001); Phys. Rev. B **65**, 045316 (2002).

<sup>6</sup> F. Li, X.-Q. Li, W.-M. Zhang, and S. A. Gurvitz, Euro. Phys. Lett. **88**, 37001 (2009).

<sup>7</sup> F. Li, H.-J. Jiao, J.-Y. Luo, X.-Q. Li, S. A. Gurvitz, Physica E **41**, 1707, (2009).

<sup>8</sup> Y. Tokura, H. Nakano, and T. Kubo, New J. Phys. **9**, 113 (2007).

- <sup>9</sup> Y.-S. Liu, H. Chen, and X.-F. Yang, *J. Phys.: Condens. Matt.* **19**, 246201 (2007).
- <sup>10</sup> D. Boese, W. Hofstetter, and H. Schoeller, *Phys. Rev. B* **66**, 125315 (2002).
- <sup>11</sup> V. Kashcheyevs, A. Schiller, A. Aharony, and O. Entin-Wohlman, *Phys. Rev. B* **75**, 115313 (2007).
- <sup>12</sup> A. Aharony and O. Entin-Wohlman, *Phys. Rev. B* **72**, 073311 (2005).
- <sup>13</sup> O. Hod, E. Rabani, and R. Baer, *Acc. Chem. Res.* **39**, 109 (2006).
- <sup>14</sup> O. Entin-Wohlman and A. Aharony, *Phys. Rev. B* **85**, 085401 (2012).
- <sup>15</sup> D. Rai, O. Hod, and A. Nitzan, *J. Phys. Chem. Lett.* **2**, 2118 (2011), *Phys. Rev. B* **85**, 155440 (2012).
- <sup>16</sup> D. Rai and M. Galperin, *Phys. Rev. B* **86**, 045420 (2012).
- <sup>17</sup> M. W.-Y. Tu, W.-M. Zhang, and J. Jin, *Phys. Rev. B* **83**, 115318 (2011).
- <sup>18</sup> M. W.-Y. Tu, W.-M. Zhang, J. Jin, O. Entin-Wohlman, and A. Aharony, *Phys. Rev. B* **86**, 11543 (2012).
- <sup>19</sup> M. W.-Y. Tu, W.-M. Zhang, and F. Nori, arXiv:1204.5931
- <sup>20</sup> S. Bedkihal and D. Segal, *Phys. Rev. B* **85**, 155324 (2012).
- <sup>21</sup> B. Kubala and J. König, *Phys. Rev. B* **65**, 245301 (2002).
- <sup>22</sup> M. Büttiker, *Phys. Rev. B* **32**, 1846 (1985); *Phys. Rev. B* **33**, 3020 (1986).
- <sup>23</sup> S. Pilgram, P. Samuelsson, H. Förster, and M. Büttiker, *Phys. Rev. Lett.* **97**, 066801 (2006).
- <sup>24</sup> H. Förster, P. Samuelsson, S. Pilgram, and M. Büttiker, *Phys. Rev. B* **75**, 035340 (2007).
- <sup>25</sup> Y. Meir and N. Wingreen, *Phys. Rev. B* **68**, 2512 (1992).
- <sup>26</sup> J. Franson, *Non-equilibrium nano-physics, a many body approach*, Lecture Notes in Physics **809**, Springer (2010).
- <sup>27</sup> A. Dhar and D. Sen, *Phys. Rev. B* **73**, 085119 (2006).
- <sup>28</sup> M. Büttiker, *Phys. Rev. B* **46**, 12485 (1992).
- <sup>29</sup> A. Batra, G. Kladnik, H. Vázquez, J.S. Meisner, L. Floreano, C. Nuckolls, D. Cvetko, A. Morgante, L. Venkataraman, *Nature Comm.* **3**, 1086, (2012).
- <sup>30</sup> I. Klich, in "Quantum Noise in Mesoscopic Systems", edited by Yu. V. Nazarov and Ya. M. Blanter (Kluwer, 2003).
- <sup>31</sup> M. G. Pala and G. Iannaccone, *Phys. Rev. B* **69**, 235304 (2004).
- <sup>32</sup> H.-P. Breuer and F. Petruccione, *The Theory of Open Quantum Systems* (Oxford University Press, Oxford, UK, 2002).
- <sup>33</sup> D. Rohrlich, O. Zarchin, M. Heiblum, D. Mahalu, and V. Umansky, *Phys. Rev. Lett.* **98**, 096803 (2007).
- <sup>34</sup> D.-I. Chang, G. L. Khym, K. Kang, Y. Chung, H.-J. Lee, M. Seo, M. Heiblum, D. Mahalu, and V. Umansky, *Nature Physics* **4**, 205 (2008).
- <sup>35</sup> A. Ueda and M. Eto, *Phys. Rev. B* **73**, 235353 (2006); *New J. of Phys.* **9**, 119 (2007); *Physica E* **40**, 1602 (2008).
- <sup>36</sup> Z. Zhu, A. Aharony, O. Entin-Wohlman, and P. C. E. Stamp, *Phys. Rev. A* **81**, 062127 (2010).
- <sup>37</sup> T. Kubo, Y. Tokura and S. Tarucha, *J. Phys. A: Math. Theor.* **43** 354020 (2010).
- <sup>38</sup> R. Härtle, M. Butzin, O. Rubio-Pons, and M. Thoss, *Phys. Rev. Lett.* **107**, 046802 (2011).
- <sup>39</sup> S. Ballmann, R. Härtle, P. B. Coto, M. Elbing, M. Mayor, M. R. Bryce, M. Thoss, and H. B. Weber, *Phys. Rev. Lett.* **109**, 056801 (2012).
- <sup>40</sup> M. Sindel, A. Silva, Y. Oreg and J. von Delft, *Phys. Rev. B* **72**, 125316 (2005).